PRINTING HIGH VISCOSITY FLUIDS USING ULTRASONIC DROPLET GENERATION

David W. Rosen, Lauren Margolin*, Sanjay Vohra
The George W. Woodruff School of Mechanical Engineering
Georgia Institute of Technology
813 Ferst Drive, Atlanta, GA, 30332-0405
(404) 894-9668, david.rosen@me.gatech.edu
*Lutron Electronics, Inc., Coopersburg, PA

ABSTRACT

A new printing technology based on ultrasonic actuation (~1 MHz) is presented that has the potential to print high viscosity fluids. In this paper, we describe the print-head's operating principles and construction. Acoustic focusing in the nozzles produces high pressure gradients that help eject the fluid which, under the proper conditions, forms droplets. Two types of models are presented to attempt to predict print-head behavior over a range of conditions. The first model borrows from simple fully developed, laminar flows to estimate printing conditions based on fluid properties, as well as printing pressures. The second model captures the dynamic behavior of the print-head to estimate cavity resonances that lead to acoustic focusing and potentially droplet generation. We report on experiments with several types of fluids that demonstrate the technology's potential.

1 INTRODUCTION

The long term objective of this project work is to deposit polymers with viscosities in the range of 1000-5000 cP in patterned 3D structures. We are taking a printing, or jetting, approach to deposit polymers as liquid droplets. If successful, this research could enable new SFF technologies and applications that require polymer materials that cannot otherwise be fabricated in general 3D structures. We favor printing technologies since they are relatively inexpensive and are scalable simply by adding nozzles. These factors are advantageous for production manufacturing applications, not simply prototyping applications.

The ink-jet printing industry is mature, with well developed printing technologies and materials. However, the industry invests heavily in the development of inks (materials) that are printable and that behave properly after printing; e.g., form images without running, splashing, etc. New printing technologies that extend the range of printable materials from the viscosity range of 1-40 cP to viscosities in the 100's or 1000's cP would be very beneficial.

A new printing technology based on ultrasonic actuation (~1 MHz) is presented in this paper that has the potential to print high viscosity fluids. Acoustic focusing in the nozzles produces high pressure gradients that help eject the fluid which, under the proper conditions, forms droplets. The print-head's operating phenomena and scaling laws are described that model its behavior over a range of conditions. Comparisons are made with the capabilities of conventional printing technologies. Experiments with several fluids that range in viscosity from 10 to 150 cP are presented and compared with predictions. It remains an open issue whether or not fluids with higher viscosities can be printed successfully.

2 JETTING TECHNOLOGIES

Generally speaking, two types of jetting modes are common: continuous mode (CM) and drop-on-demand (DOD). In continuous mode jetting, an unbroken jet of fluid projects from an orifice; Rayleigh instabilities cause the jet to break up into individual droplets after a certain flight distance. In demand mode, individual droplets are ejected from an orifice, usually as a result of a pulsed energy source.

Various types of jetting heads have been developed for various types of materials and deposition requirements. Of interest here are piezoelectric actuators that eject material through a nozzle. These piezoelectric actuators can be used for either continuous or demand mode of printing. Operating principles can be either electromechanical pumping of the fluid or thermally driven pumping. Bubble-jet technologies use the latter approach, heating the water-based ink until the water vaporizes and using the vapor pressure to cause a droplet to be ejected. A very large body of literature exists on the various aspects of printing [9], including many papers over the past 20 years on printing of polymers [8], metals [10], and ceramics [23].

MicroFab Technologies [17] is a well known supplier of jetting equipment that supplies heads using piezoelectric actuation. Their print-heads utilize the pumping principle. Typical operating frequencies are 2 – 20 kHz. In addition, it is common to heat print-heads and the fluid being printed, since fluid viscosity often decreases as the temperature is increased. At the printing temperature, fluids with viscosities between 1 – 40 mPa·s (centi-Poise, cP) and surface tensions 0.02 – 0.5 N/m can be printed typically through nozzle sizes ranging from 100 to 30 μm [23]. Other companies, such as Dimatix (www.dimatix.com) and Xaar (www.xaar.co.uk), produce print-head arrays with up to 1000 nozzles. Their operating frequencies, temperatures, and printable viscosities and surface tensions are similar to those of MicroFab.

In the SFF industry, several good examples of jetting technology have been incorporated into commercial machines. Sanders Inc. was the first company to commercialize this technology (www.solidscape.com), using two jetting nozzles, one for a wax-based part material and the other for support structure. 3D Systems (www.3dsystems.com) introduced two jetting machines that fabricated parts in a wax material, the Actua 2100, introduced in 1997, and the ThermoJet, in 2001. Resolutions of 300 to 600 dpi are possible.

In 2003, 3D Systems introduced their Invision machine that printed a photopolymer to define each cross-section of a part. After printing a cross-section, a UV lamp was flashed to cure the photopolymer. A special support structure material ensured that complex shapes could be built in the Z direction. In 1999, the Israeli company Objet (www.2objet.com) introduced a machine with several hundred nozzles. Current Objet machines have 1500 nozzles and are capable of building in two part materials (and mixtures). The photopolymer materials used in these machines are acrylates, which do not have
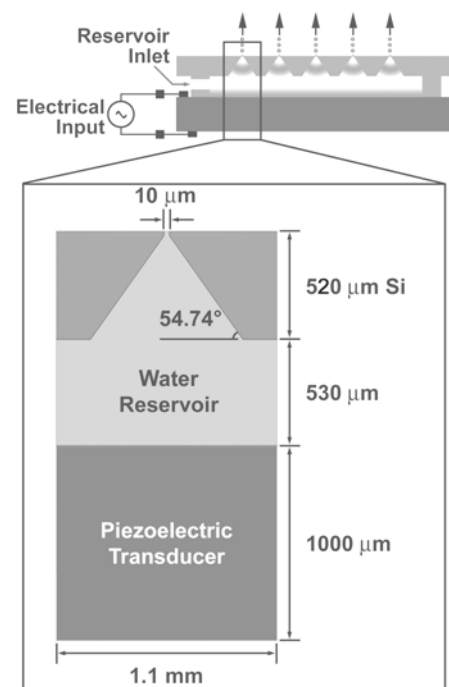

Fig. 1. Schematic of the ultrasonic droplet generator with representative dimensions.

desirable mechanical properties for most production applications and which age, limiting their usefulness to prototype parts.

In the early 1990's, researchers at MIT developed the 3D Printing (3DP) technology that involves printing binder into a powder bed [22]. Although 3DP may benefit from printing technologies capable of high viscosity fluids, our primary interest is in printing part material, not binder, so 3DP will not be considered further in this paper.

3   GEORGIA TECH ULTRASONIC DROPLET GENERATOR

3.1   Operational Principles

Jetting technologies based on ultrasonic actuation have received considerable attention in the past several years, although the foundations were developed in the mid-1980's [7]. Femptoliter (fl) sized droplets were produced by de Heij *et al.* [1] and by Ederer *et al.* [6] using piezoelectrically actuated ejectors with arrays of micromachined nozzles etched through thin membranes. These droplet generators were limited to submegahertz operation. Perçin *et al* [19-21] presented a technique for ejecting liquids using a micromachined flextensional ultrasound transducer to excite axisymmetric resonant modes in a clamped circular plate. Ejection of low viscosity fluids was demonstrated for a number of orifices, including a 4 μm orifice in a 100 μm dia. membrane driven at 3.45 MHz. However, complex manufacturing procedures were necessary to fabricate printing heads, limiting their practical application.

A new Georgia Tech ejector utilizes cavity resonances in the 1-5 MHz range along with the acoustic wave focusing properties of a liquid horn structure to generate the pressure gradient required to form and eject a droplet [15]. A schematic of this concept is in Figure 1. The thickness of the piezoelectric transducer is chosen so that its resonance matches the cavity resonance. When the piezoelectric transducer is driven at the resonant frequency of the fluid chamber (dictated by the horn structure and the transducer itself), constructive interference due to the shape of the horn structure focuses the acoustic waves towards the nozzle. As a result, a standing acoustic wave develops with the peak pressure gradient occurring near the tip of the nozzle (Figure 2), which provides a circumstance for low power droplet ejection.
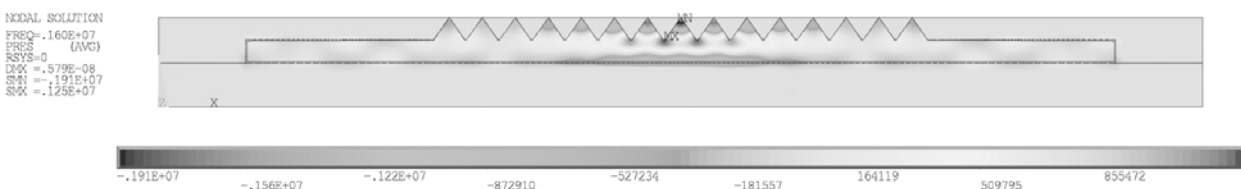

Fig. 2. Real components of the complex representations of the acoustic pressure fields in water for the middle of three resonant modes that result in pressure wave focusing at the nozzle tips.

3.2   Ejector Fabrication Process

The print-head device comprises a fluid reservoir that is formed between a bulk ceramic piezoelectric transducer and an array of liquid horn structures wet etched into silicon. The main component in the print-head is the nozzle plate, with an array of nozzles. Although a number of nozzle shapes are capable of focusing acoustic waves, the pyramidal shape was chosen as it can be readily established via a single step potassium hydroxide (KOH) wet etch of (100) oriented silicon [11]. The size of the square feature representing the base of the pyramid is designed so

241

that the focusing horns terminate near the opposite side of the ejector plate. An inductively coupled plasma (ICP) dry etch is then used to open the orifices from the back side. A 2 μm thick silicon oxide "hard mask" was used to pattern the nozzle holes for ICP, which resulted in successful fabrication of nozzles as small as 3-4 μm in diameter. Note that this two step fabrication process represents a significant improvement over the complexity inherent in other ultrasonic ejector designs [15,16].

In the first generation of droplet generators, PZT-8 ceramic was used for the piezoelectric transducer. The reported longitudinal acoustic wave velocity characteristic of PZT-8 is used to estimate the piezoelectric thickness that is required to place the transducer resonance within the envelope of cavity resonances, which are dictated by the liquid horn structure, the speed of sound within the ejection fluid, and the cavity size itself [15,16]. For our experiments to date, the transducer was assembled with a spacer and a nozzle array as shown in Fig. 1.

3.3 Print-Head Device Design

The design of the final assembly is shown in Figure 3 [12]. The black square in the center of the top surface is the nozzle array; the droplets are ejected vertically from it. The main concept of this system is that of a sandwich, where the piezoelectric element and the nozzle array are held together between lower and upper parts of a housing, which also provides the electrical and fluid interfaces for the system. The main body was built in a Viper Si2 stereolithography machine (3D Systems, Valencia CA) using SOMOS 10120 resin (DSM Somos, New Castle DE); this method of manufacture provides numerous advantages. Because it is an additive process, detail and contouring of internal fluid pathways is easily achieved and is exploited in this design. Additionally, the transparency of the build material allows visual confirmation of the placement of nozzle array and spacer, even after the housing is assembled. Other internal aspects of the process, such as fluid filling and flow, can be visually monitored with this SLA housing.

The upper housing has a protective 'pocket' for the nozzle array; a gasket between them forms a liquid barrier and cushions the nozzle array. The other side of the nozzle array is adjacent to the spacer, which is made of a compliant but incompressible aramid/Buna-N gasket covered with Kapton tape. Selection of a compliant material also reduces stresses on the nozzle array that occur when it is compressed against harder, possibly irregular surfaces, thus preventing breakage.

The piezoelectric transducer is attached to the lower housing, and the two electrical leads are soldered directly to the top and bottom of the piezoelectric element. The lower housing also has stiffening bars that prevent warpage when the connectors are tightened in the corners. This allows a uniform pressure on the interior components, which is another method of preventing nozzle array breakage.

3.4 Ejection System

The experimental facility that was developed for visualization of the ejection process is shown in Figure 4 [16]. The piezoelectric transducer is driven by an AC voltage signal at the resonant frequency of the fluid cavity. This signal is generated by the function generator labeled "Function Generator 1" and then amplified (RF Amplifier). An
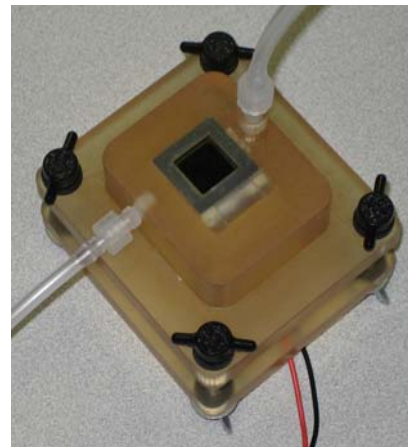

Figure 3. Printing nozzle assembly.

oscilloscope is used to monitor the voltage signal applied to the piezoelectric transducer.

We have developed a stroboscopic system to visualize droplet ejection. The system uses pulsed Ultra-bright LEDs to strobe the light on the droplets at a frequency synchronized with ejection and a CCD camera records these frozen images.

3.5 Ejector Characterization

Figure 5 shows ejection of 4μm diameter water droplets from a 3.8μm diameter nozzle at 916 kHz. Since each image is a superposition of approximately 100,000 exposures, the figure shows the stability of the ejection process. One can also estimate the speed of the droplets since the time difference between droplets is one period of the driving sinusoidal signal. Our next goal for this project is to generate one drop at a time using tone burst excitation in order to achieve DOD mode ejection. That is, we want to demonstrate true DOD mode ejection, not just droplet ejection.

Figure 4. Schematic of the ejection and visualization system.

We used a laser based Phase Doppler Particle Analyzer (PDPA) system to measure the distribution of droplet size and droplet velocity at different distances from the nozzles. As expected, the droplet size has a tight distribution when the substrate is close to the nozzle (1mm away) and the average droplet velocity is high (as large as 10-15 m/s). As the distance is increased to 10mm, droplet size reduces due to evaporation, and the velocity is reduced, as expected. The temperature of the piezoelectric transducer was measured during these experiments. The transducer temperature never exceeded 50ºC even when all ejectors on a 200 nozzle ejector plate were active, with water as the fluid. Temperature will depend on the properties of the fluid ejected, and it needs to be monitored during future printing experiments with various manufacturing materials.

4 MODELS OF THE PRINTING PROCESS

4.1 Fluidics Modeling

While the liquid to be ejected travels through the nozzle, before forming droplets, its motion is governed by the standard equations for incompressible, Newtonian fluids, as we are assuming these flows to be. The flow is fully described by the Navier-Stokes and continuity equations; however, these equations are difficult to solve analytically, so we will proceed with a simplification. The first term on the right side of Eqn. 2 takes advantage of one situation for which an analytical solution is possible, that of steady, incompressible, laminar flow through a
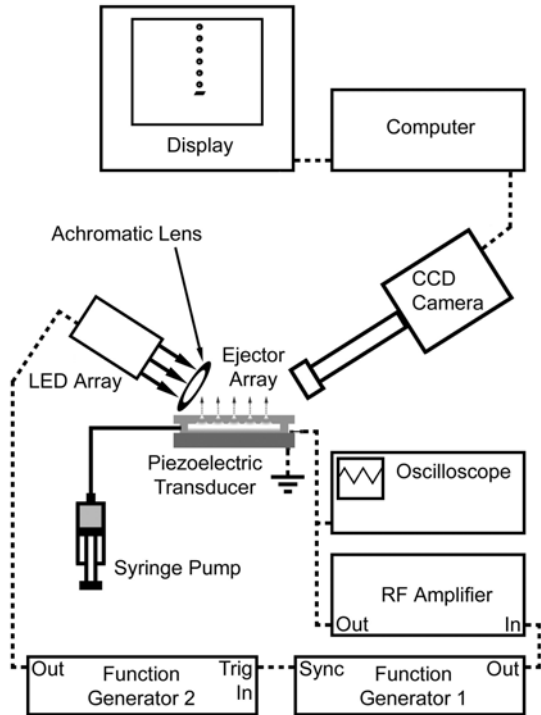

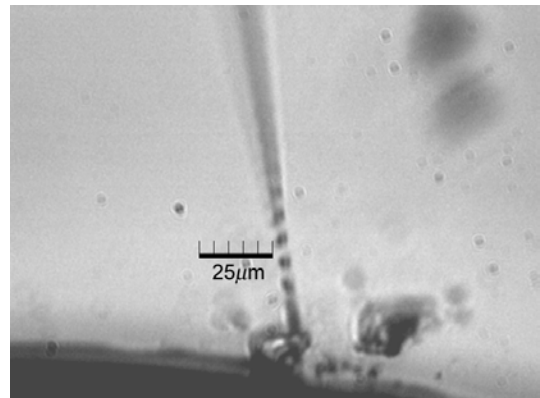Figure 5. Stroboscopic imaging of water droplet ejection at 0.92 MHz from a 3.8μm diameter nozzle.

straight circular tube of constant cross section. The solution is the Hagen-Poiseuille law [18], which reflects the viscous losses due to wall effects:

$$\Delta p = \frac{8Q\mu l}{\pi r^4}$$ (1)

where, Δp is the total gauge pressure required, μ is the dynamic viscosity of the liquid, l is the length of the nozzle or supply tubing, Q is the flow rate, and r is the tube radius. Note that this expression is most applicable when the nozzle is a long, narrow glass tube. However, it also applies when the fluid is viscous, as we will see shortly.

Another assumption made by using the Hagen-Poiseuille equation is that the flow within the nozzle is fully developed. For the case of laminar flow in a cylindrical pipe, the length of the entry region l_e where flow is not yet fully developed is defined as 0.06 times the diameter of the pipe, multiplied by the Reynolds number [18]:

$$l_e = 0.06d \, \text{Re} = \frac{0.06\rho\bar{v}d^2}{\mu}$$ (2)

where $\bar{v}$ is the average flow velocity across the pipe, ρ is the liquid's density, and $d = 2r$. In order to appreciate the magnitude of this effect, consider printing with a 20 μm nozzle in a plate that is 100 μm thick, where the droplet ejection speed is 10 m/s. The entry lengths for a fluid at various viscosities and two densities are shown in Table 1.

Table 1. Entry lengths for fluid at several viscosities.

Viscosity (cP)	Density (kg/m^3)	Entry Length (μm)
1	1000	240
	1250	300
10	1000	24
	1250	30
40	1000	6
	1250	7.5
100	1000	2.4
	1250	3
200	1000	1.2
	1250	1.5

Entry lengths are a small fraction of the nozzle length for fluids with viscosities of 40 cP or greater. As a result, we can conclude that flows are fully developed through most of a nozzle for fluids that are at the higher end of the range of printable viscosities.

Fluid flows when printing are almost always laminar; i.e., the Reynolds number is less than 2100. The Reynolds number is Eqn. 3. Another dimensionless number of relevance in printing is the Weber number (Eqn. 4), which describes the relative importance of a fluid's inertia compared to its surface tension, γ, at flow velocity v.

$$\text{Re} = \frac{\rho v r}{\mu}$$ (3) $$We = \frac{\rho v^2 r}{\gamma}$$ (4)

Several research groups have determined that a combination of the Reynolds and Weber numbers is a particularly good indication of the potential for successful printing of a fluid [23]. Specifically, if the ratio of the Reynolds number to the square root of the Weber number has a value between 1 and 10, then it is likely that ejection of the fluid will be successful. This condition will be called the "printing indicator" and is:

$$1 \leq \frac{\text{Re}}{We^{1/2}} = \frac{\sqrt{\rho r \gamma}}{\mu} \leq 10 \tag{5}$$

The inverse of the printing indicator is another dimensionless number called the Ohnsorge number, that relates viscous and surface tension forces. Note that low values of this ratio indicate that flows are viscosity limited, while large values indicate flows that are dominated by surface tension. The low value of 1 for the printing indicator means that the maximum fluid viscosity should be between 20 and 40 cP, where the viscosity range covers the ranges of densities and surface tensions for typical fluids.

4.2 Acoustic Field Model

In ultrasonic droplet generation, ejection of droplets occurs when the pressure gradient in the nozzle imparts enough energy to the liquid within the nozzle to overcome viscous forces and fluid inertia. Large pressure gradients are caused by focusing of acoustic energy which is maximized when a standing wave is formed in the fluid cavity [14]. Such a standing wave is formed when the distance between the piezo and the nozzle tip region is ½ wavelength, 1 wavelength, or a harmonic. This simple situation is complicated in practice since the acoustic field is influenced by neighboring nozzles, nozzle shape and size, reflections off of other surfaces, mechanical properties of the fluid and of the device components, etc. As a result, it is important to understand print-head dynamics over a range of input frequencies to identify cavity resonances (when standing waves form) and piezo resonances.

First order approximations of fluid cavity and piezo responses lend some insight. The fundamental resonant frequency of the nozzle cavity is a function of cavity height, h_n, and the speed of sound in the fluid, c [14].

$$f_n \approx \frac{c}{2h_n} \tag{6}$$

For the case of printing water with a 0.5 mm spacer ($h_n = 0.995$ mm) and speed of sound of 1500 m/s, the first two resonant frequencies are 0.754 MHz and 1.508 MHz, respectively. For glycerin with a 0.84 mm spacer and a speed of sound of 1900 m/s, expected resonant frequencies are 0.955 MHz and 1.91 MHz, respectively.

The natural resonant frequency of the piezoelectric element depends on its material, geometry, and dimensions. For a flat plate transducer, the resonant frequency f_p is defined by the equation

$$f_p = \frac{N_T}{h_p} \tag{7}$$

where N_T is the thickness mode frequency constant and h_p is the thickness of piezoelectric element. For the piezoelectric material used here, APC 880 (APC International, Mackeyville PA), $N_T = 2110$ m/s. Thus for a transducer of thickness 1.5 mm, as used in this research, the

resonant frequency is calculated at 1.41 MHz. The piezo resonance is typically chosen to lie between the first and second cavity resonances, and is usually closer to the second.

Acoustic simulations were performed using the harmonic response analysis capabilities of ANSYS over the frequency range (0.3–2.8 MHz) of interest. This analysis solved the second order (in time) equations of motion governing the structural response of the silicon and the acoustic response of the fluid chamber, and the mixed order (e.g., electrical and structural) equations governing the dynamics of the piezoelectric transducer. All loads and displacements were assumed to vary sinusoidally at the same known frequency.

Results of the harmonic analysis included a graph of electrical input impedance vs. driving frequency. Resonant modes of the print-head are identified by spikes in the graph (either the real or imaginary parts of impedance). Piezo resonance is also indicated by a spike, so care is needed to distinguish spikes that are potential frequencies for ejection from other system resonances. Very good agreement was demonstrated between the ANSYS simulations and measurements during dynamic response experiments using a network analyzer [14], lending confidence in the simulation's capability to provide useful information when planning ejection experiments.

Results of one simulation are shown in Figure 6 for a print-head with a 0.84 mm spacer and glycerin as the fluid (density = 1250 kg/m^3). The first three cavity resonances are labeled with numbered circles, while the piezo resonance is labeled as f_p. The first and second cavity resonances from Figure 6 are at approximately 0.92 MHz and 1.67 MHz, respectively, reasonably close to the predictions from Eqn. 6 of 0.955 MHz and 1.91 MHz. Several characteristics of the simulated performance should be noted. First, predicted cavity resonances typically overestimate the actual resonance due to viscous losses in the fluid, the formation of boundary layers along the nozzle surfaces, etc. Second, higher harmonics tend to be closer to the lower harmonics than predicted. In this case, the first cavity resonance was overpredicted by 0.035 MHz (0.955 - 0.92), while the second resonance was off by 0.24 MHz. Finally, the piezo resonance falls between the first and second cavity resonances and is closer to the second.
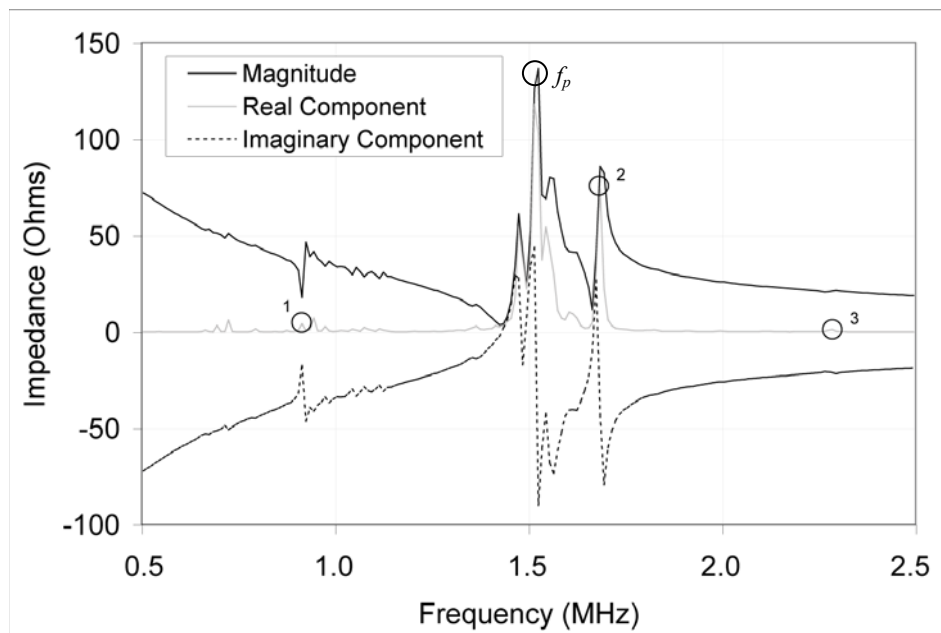

Figure 6 Print-head response for glycerin.

246

From this simulation, the region of frequencies close to the second cavity resonance should provide the best droplet ejection capability, compared to the first and third cavity resonances. The second resonance peak is high, fairly wide, and is close to f_p, all of which are favorable to ejection, based on experience with this printing technology.

5 PRINTING TEST RESULTS

Two sets of experiments were performed to test the ultrasonic droplet generation technology. The first experiment set was performed on four different classes of materials on an older print-head (nozzle plate described in Section 3.2). The second set was performed using the print-head described in Section 3.3 and included only glycerol solutions under a wide range of process conditions.

5.1 Experiment Set 1

Three families of materials were tested on the ultrasonic acoustic resonance jetting setup: polydimethylsiloxanes (Alfa Aesar Ward Hill, MA; Dow Corning, Midland, MI) [2], aqueous glycerol solutions (Fisher Scientific, Fair Lawn, NJ) [4], and aqueous polyethylene glycol (Alfa Aesar, Ward Hill, MA) solutions [3]. These were selected as relatively common experimental fluids with documented properties and few safety hazards. As a representative material of interest, the photopolmerizable DSM Somos WaterClear 10102 stereolithography resin [5] was also tested. These four materials have viscosities up to 600 cP at room temperature and surface tensions covering almost the entire range of values found in practice. Surface tensions were assumed constant as they vary only a few percent over the relevant viscosity ranges.

Printing results are presented in Table 2 with the following values:

Nominal Viscosity = viscosity as mixed at ambient conditions
Jettability = measure of how well the material ejects:
      0 = no jetting
      1 = no jetting, but pre-jetting bubbling and excitation
      2 = jetting
Frequency = frequency or range of frequencies at which piezo is driven during best ejection or excitation
Temperature = temperature seen at piezo during best ejection or excitation
Adj. Viscosity = viscosity (adjusted) of material at temperature listed

The polydimethylsiloxane (PDMS) samples were mixed from 50cS and 500cS fluids in appropriate ratios to achieve the desired viscosity. Surface tension was taken as 0.021 N/m. The stereolithography resin, DSM Somos Waterclear 10120, was tested in its standard form as provided by DSM Somos. Its viscosity vs. temperature relationship was not known. Its surface tension was measured as 0.038 N/m. The polyethylene glycol (PEG) solutions were mixed from varying ratios of water and polyethylene glycol solids. Glycerol solutions were prepared similarly. Surface tensions for these two solutions were 0.052 N/m and 0.065 N/m, respectively.

Operating temperatures were not available during the glycerol tests. During subsequent attempts to measure these temperatures, ejection results were not repeatable. It is important to realize that the adjusted viscosity values for glycerol and SOMOS 10120 are not correct.

The PDMS, PEG, and SOMOS materials were all tested with a print-head with a 2.5 mm thick piezo. According to Eqn. 7, the resonant frequency of this piezo is 0.844 MHz. From the

results in Table 2, it appears that ejection, whether printing or bubbling, was achieved at or near the piezo resonant frequency, rather than at a cavity resonance. Harmonic analysis confirmed the cavity and piezo resonances. Excessive heating of the fluid occurs when the print-head is driven at the piezo resonance. As a consequence, it can be assumed that the fluid is heated until the viscosity drops enough to enable ejection.

Table 2. Printability Results

Nominal Viscosity (cP)	Frequency (Mhz)	Temperature (°C)	Adj. Viscosity[1] (cP)	Jettability
Polydimethylsiloxane				
50	0.835	70	28	1
100	0.830	80	46	1
200	0.800-0.900	60	131	1
400	0.750-0.900	60	262	1
SOMOS 10120				
130	0.845	65	130	2
Polyethylene Glycol				
80	0.850	85	15	2
200	0.840	60	90	1
300	0.850	90	45	2
500	0.840-0.850	40	300	1
Glycerol				
15	1.445	-	15*	2
110	1.445	-	110	2
220	1.464	-	220	2
310	1.470	-	310	2
625	1.470	-	625	2

* viscosity values for glycerol could not be adjusted since temperature was not measured. Viscosities are lower than reported.
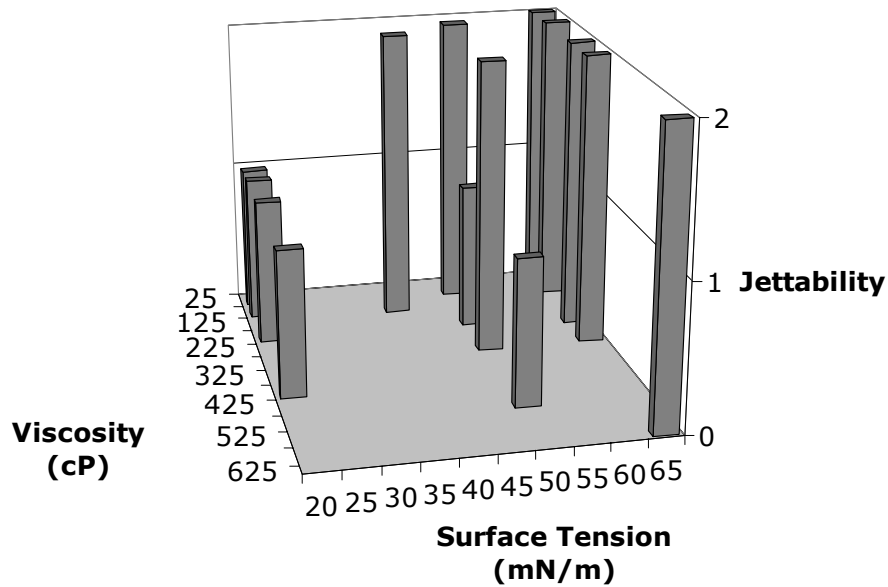

Figure 7. Cumulative Results

---

[1] Estimated from viscosity temperature coefficient.

Cumulative results: Results for all the materials can be seen together in Figure 7. As a general trend, materials with high surface tension and low viscosity were the most likely to eject, whereas materials with low surface tension and high viscosity were the least likely to eject. Based on these results, it is not clear that the ultrasonic printing technology is capable of ejecting fluids with viscosities significantly higher than the range of 1 to 40 cP.

5.2 Experiment Set 2

The testing reported here was intended to address a wide range of process circumstances and, specifically, to investigate the relationship between the nozzle cavity resonances and the resonance of the piezoelectric transducer itself. The redesigned jet-head was used, along with a piezoelectric element that was 1.5 mm thick, the spacer was 840 μm thick, and the nozzle array was 500 μm thick and had orifices that were 16 μm in size.

The experiments reported here involved the jetting of glycerol solutions. Although a wide range of frequencies was investigated in this testing, ejection was witnessed only at three frequencies: the first and second cavity resonances and the piezoelectric transducer's resonance, the frequency of which falls between the prior two resonances. No ejection was seen at the third cavity resonance. Table 3 provides details about the performance observed with these materials. For each of the materials and each of the three resonances at which ejection was seen, the frequency at which the qualitatively best ejection was seen, the lowest temperature at which ejection was possible, and the calculated viscosity at that temperature are given.

Table 3. Aqueous Glycerol Solutions Test Results

Sample #	Viscosity at Room Temp. (cP)	Best Ejection Frequency (MHz)	Operating Temperature (°C)	Viscosity at Operating Temp. (cP)	Result	Printing Indicator (Eqn. 4)
First Cavity Resonance						
1	15	0.97	34	9	2	3.87
2	110	--	--	--	1	
3	220	0.99	51	34	2	1.05
4	310	--	--	--	1	
5	625	0.99	60	45	2	0.801
Piezoelectric Transducer Resonance						
1	15	1.42	47	5	2	6.97
2	110	1.47	50	21	2	1.70
3	220	1.47	50	36	2	0.996
4	310	1.46	66	23	2	1.56
5	625	1.47	65	38	2	0.949
Second Cavity Resonance						
1	15	1.63	32	9	2	3.87
2	110	1.65	43	30	2	1.19
3	220	1.65	50	36	2	0.996
4	310	1.66	40	78	2	0.460
5	625	1.63	40	142	2	0.254

The cavity resonances determined experimentally in Table 3 correspond well with those predicted using harmonic analysis and reported in Figure 6: 0.92 vs. 0.97-0.99 MHz and 1.67 vs. 1.63-1.66 MHz. Similarly, piezo resonance was predicted at 1.41 MHz (Eqn. 7) and observed at 1.42-1.47 MHz.

It is notable that at the first cavity resonance, which is quite far from the transducer's resonant frequency, ejection was observed to be somewhat weak and unreliable; this is confirmed by the data in Table 3, which shows that two of the samples did not eject at all at that resonance.

Also notable is the heating that occurred when driving the system at the piezo resonant frequency. Operating temperatures were up to 26 °C higher at the piezo resonance, compared to the second cavity resonance. This indicates the advantage of acoustic focusing in the nozzle compared to reliance on piezo or other system resonances to cause ejection. It also indicates the inefficiency associated with driving the piezo at its resonant frequency.

In comparison with Eqn. 5, the printing indicator, samples 4 and 5 at the second cavity resonance clearly demonstrate the capability of printing outside of the generally accepted parameter ranges. These results demonstrate the potential for ultrasonic droplet generation technology to be applied for viscous fluids.

6   HIGH VISCOSITY FLUIDS

We discuss the potential of the ultrasonic droplet generation technology to print high viscosity fluids. It is clear that current "printability" guidelines do not apply well, yet no other guidelines are available that indicate limits on printability. Comments on viscous damping and ejection pressures will be presented in this section.

One basic principle that is instructive in the case of jetting is that of conservation of energy. The energy imparted by the actuation method to the liquid must be sufficient to balance three requirements: fluid flow losses, surface energy, and kinetic energy, as expressed in Eqn. 8.

$$E_{imparted} = E_{loss} + E_{surface} + E_{kinetic} \qquad (8)$$

The losses originate from a conversion of kinetic energy to thermal energy due to the viscosity of the fluid within the nozzle; this conversion can be thought of as a result of internal friction of the liquid. The surface energy requirement is the additional energy needed to form the free surface of the jet or droplets [13,16]. Finally, the resulting jet or droplets must still retain enough kinetic energy to propel the liquid from the nozzle towards the substrate. Analysis has shown that of the energy terms on the right side of Eqn. 8, the viscous loss term dominates in typical cases and is very dominant at high viscosities (above 100 cP) [12].

To quantify aspects of the viscous losses, consider the Hagen-Poiseuille law introduced in Eqn. 1. Assumptions related to this law include fully developed flow, which was demonstrated in Sec. 4.1, as well as steady and laminar flow. For a vibrating actuator, the flow will actually be oscillatory, which is a limitation of this analysis. Nonetheless, the Hagen-Poiseuille law will be used to estimate the pressure required to eject fluid of 500 cP viscosity as a function of orifice diameter (density = 1000 kg/m^3, surface tension = 0.072 N/m).

Pressures required to eject this fluid at various orifice diameters and for three different flow lengths are plotted in Figure 8. At diameters smaller than 0.06 mm, pressures increase significantly, indicating the difficulty in ejecting viscous fluids through small orifices. Flow lengths are difficult to estimate. Nozzles are pyramidal in shape, but end in a straight section of square cross-section, usually only several μm in length. As noted in Table 1, flows are fully developed after 1-3 μm of flow length for viscous fluids. If the effective length of flow with wall friction losses is less than 10 μm, then pressures are below 20 MPa for even the smallest

orifices. However, if the effective flow length is closer to the thickness of the nozzle plate (0.5 mm), then pressure drops will be very high. Acoustic focusing leads to high pressure gradients that can amplify pressures by at least an order of magnitude, as shown in Figure 2. Hence, line pressures of 1 to 5 MPa should be sufficient to eject 500 cP fluid through 0.04 mm orifices, if not smaller.
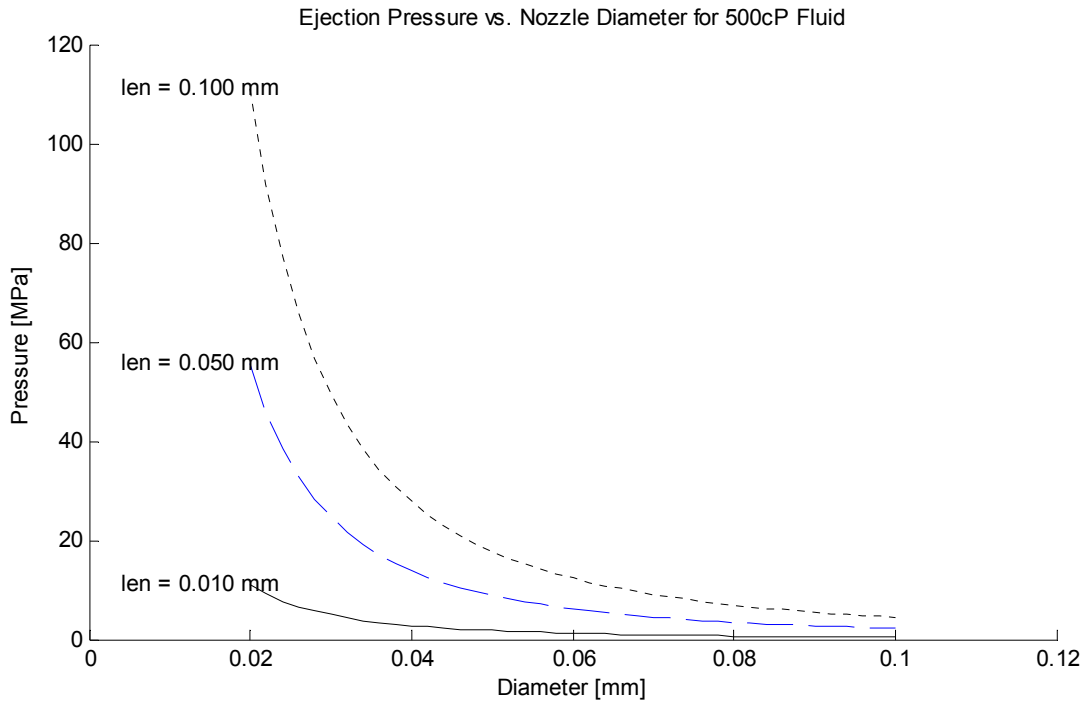

Figure 8. Variation of ejection pressure as a function of orifice diameter.

7   CONCLUSIONS

A new printing technology based on ultrasonic actuation (~1 MHz) was presented that demonstrated the capability of printing fluids with higher viscosities than conventional print-heads. Acoustic focusing in the nozzles produces high pressure gradients that help eject the fluid which, under the proper conditions, forms droplets. A fluid mechanics model was presented that estimated printing conditions based on fluid properties, as well as printing pressures. A second dynamics model estimated cavity resonances that could lead to acoustic focusing and potentially droplet generation. Two sets of experiments were reported with several types of fluids that demonstrate droplet generation under a wide range of conditions.

Specific conclusions based on this work include:

- acoustic focusing at ultrasonic driving frequencies can cause ejection of high viscosity fluids, up to 150 cP,

- viscous losses are the most significant impediment to droplet generation in high viscosity fluids,

- driving the piezo at the second cavity resonance tends to provide better results that at other cavity resonances, particularly when the second resonance is close to the piezo resonant frequency,

- fluids with higher surface tension tend to be easier to eject than fluids with lower surface tensions.

A significant amount of research remains in order to realize the potential of ultrasonic droplet generation technology for printing engineering fluids for SFF applications. Many fluids of interest have viscosities between 100 - 1000 cP at printing temperatures. In order to improve the technology, a better understanding of print-head dynamics and acoustic focusing is needed. Harmonic analyses must be augmented with models of viscous losses. Additionally, droplet generation needs to be simulated using high fidelity CFD methods [12,14] for high viscosity fluids to predict conditions at which droplet generation may be possible.

REFERENCES

[1] de Heij, B., van der Schoot, B., Bo, H., Hess, J., and de Rooij, N. F., "Characterization of a fL droplet generator for inhalation drug therapy," *Sensors and Actuators, A: Physical*, vol. 85, pp. 430-434 (2000).

[2] Dow Corning (2002), "Blending chart for Dow Corning 200 Fluid."

[3] Dow Chemical (2002). "Carbowax PEGS & MPEGS.".

[4] Dow Chemical Company. "DOW Glycerine: Physical Properties". Accessed August 23, 2006 from <http://www.dow.com/glycerine/resources/physicalprop.htm>.

[5] DSM Somos. "Somos Waterclear 10120 Product Data Sheet". Accessed August 29, 2006 from <www.dsm.com/en_US/downloads/ dsms/somos10120product_data_sheet.pdf>.

[6] Ederer, I., Raetsch, P., Schullerus, W., Tille, C., and Zech, U., "Piezoelectrically driven micropump for on-demand fuel-drop generation in an automobile heater with continuously adjustable power output," *Sensors and Actuators, A: Physical*, vol. 62, pp. 752-755 (1997).

[7] Elrod, S. A., Hadimioglu, B., Khuri-Yakub, B. T., Rawson, E. G., Richley, E., Quate, C. F., Mansour, N. N., and Lundgren, T. S., "Nozzleless droplet formation with focused acoustic beams," *Journal of Applied Physics*, vol. 65, pp. 3441-3447 (1989)

[8] Gao, F. and Sonin, A. A. (1994). "Precise deposition of molten microdrops: the physics of digital fabrication." Proceedings of the Royal Society of London (A), 444, 533-54.

[9] Lee, E.R., *Microdrop Generation*, CRC Press LLC, Boca Raton, FL, 2003.

[10] Liu, Q. and Orme, M. (2001). "High precision solder droplet printing technology and the state-of-the-art." *Journal of Materials Processing Technology*, 115, 271-83.

[11] Madou, M. J., *Fundamentals of Microfabrication*. CRC Press, LLC, Boca Raton, FL, USA, 2002.

[12] Margolin, L. (2006), "Ultrasonic Droplet Generation Jetting Technology for Additive Manufacturing: An Initial Investigation," MS Thesis, Georgia Institute of Technology.

[13] McKinley, G. (2005). "Dimensionless groups for understanding free surface flows of complex fluids." Department of Mechanical Engineering, Massachusetts Institute of Technology.

[14] Meacham, J. M. (2006). "A micromachined ultrasonic droplet generator: design, fabrication, visualization, and modeling," Ph.D. dissertation, Georgia Institute of Technology.

[15] Meacham, J.M., C. Ejimofor, S. Kumar, F. L. Degertekin, and A. G. Fedorov, "A Micromachined Ultrasonic Droplet Generator Based on a Liquid Horn Structure," *Review of Scientific Instruments*, 75, pp. 1347-1352, 2004.

[16] Meacham, J. M., Varady, M. J., Degertekin, F. L., and Fedorov, A. G., "Droplet formation and ejection from a micromachined ultrasonic droplet generator: Visualization and scaling," *Physics of Fluids*, Vol. 17, Issue 10, October (2005).

[17] "MicroFab technote 99-01: Background on ink-jet technology". Accessed March 19, 2006 from <http://www.microfab.com/equipment/technotes/technote99-01.pdf>

[18] Munson, B., Young, D. and Okiishi, T. (1998). *Fundamentals of Fluid Mechanics* (3rd ed.). New York: John Wiley and Sons.

[19] Perçin, G. and Khuri-Yakub, B. T., "Micromachined droplet ejector arrays for controlled ink-jet printing and deposition," *Review of Scientific Instruments*, vol. 73, pp. 2193-2196 (2002).

[20] Perçin, G. and Khuri-Yakub, B. T., "Piezoelectrically actuated flextensional micromachined ultrasound droplet ejectors," *IEEE Transactions on Ultrasonics, Ferroelectrics, and Frequency Control*, vol. 49, pp. 756-766 (2002).

[21] Perçin, G., Yaralioglu, G. G., and Khuri-Yakub, B. T., "Micromachined droplet ejector arrays," *Review of Scientific Instruments*, vol. 73, pp. 4385-4389 (2002).

[22] Sachs, E., M. Cima, P . Williama, D. Brancazio, J. Cornie, "Three Dimensional Printing: Rapid Tooling and Prototypes Directly from a CAD Model," *ASME Journal of Engineering for Industry*, Vol. 114, pp. 481-8, 1992.

[23] Seerden, KAM, Reis, N, Evans, JRG, Grant, PS, Halloran, JW, Derby, B, "Ink-Jet Printing of Wax-Based Alumina Suspensions," *J. American Ceramics Society*, 84(11):2514-20, 2001.